CHAPTER IV
RESULTS AND DISCUSSION

4.1 Static Adsorption of *m*- and *p*-CNB

4.1.1 Single Component Adsorption

The singular adsorption behaviors of *m*-CNB and *p*-CNB on zeolites, MgX, CaX, SrX, BaX, MgY, CaY, SrY, and BaY, were studied. The di-valence ion exchanged faujasite zeolites were calcined at 350°C for an hour prior to the experiment. The adsorption capacities of *m*-CNB and *p*-CNB on FAU zeolites are shown in Figures 4.1–4.16.

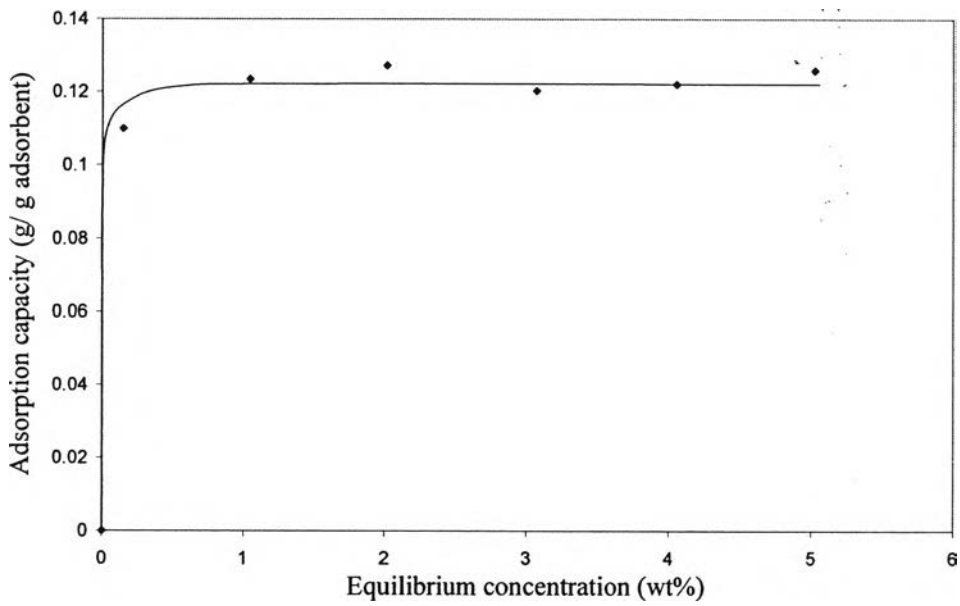

Figure 4.1 Adsorption isotherm of *m*-CNB on MgX at 30°C.

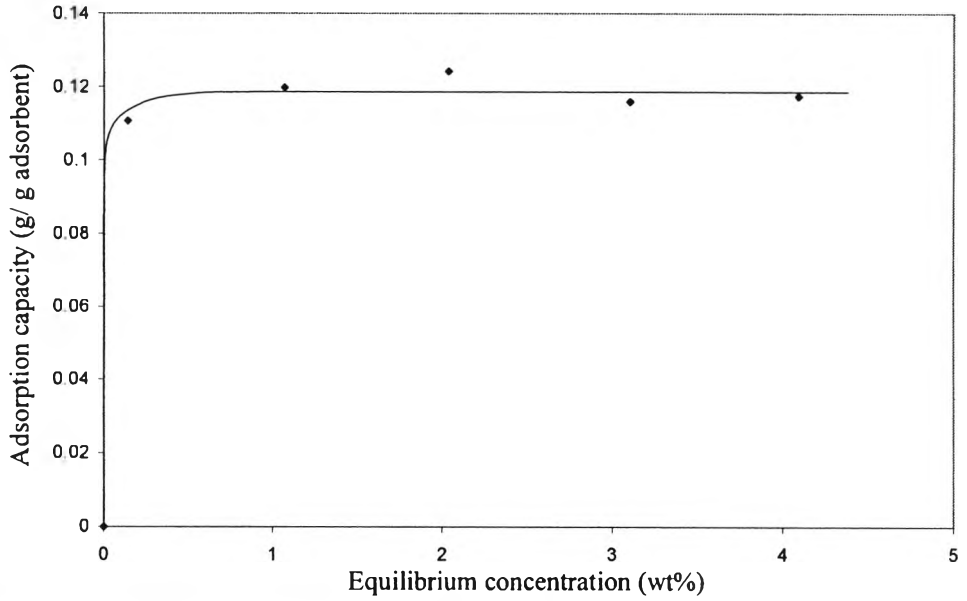

Figure 4.2 Adsorption isotherm of *p*-CNB on MgX at 30°C.

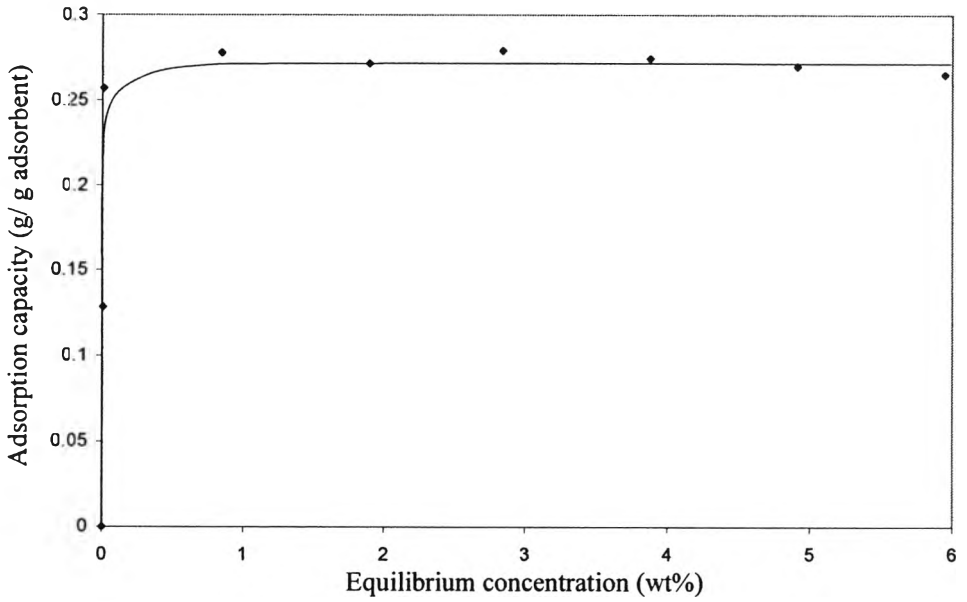

Figure 4.3 Adsorption isotherm of *m*-CNB on CaX at 30°C.

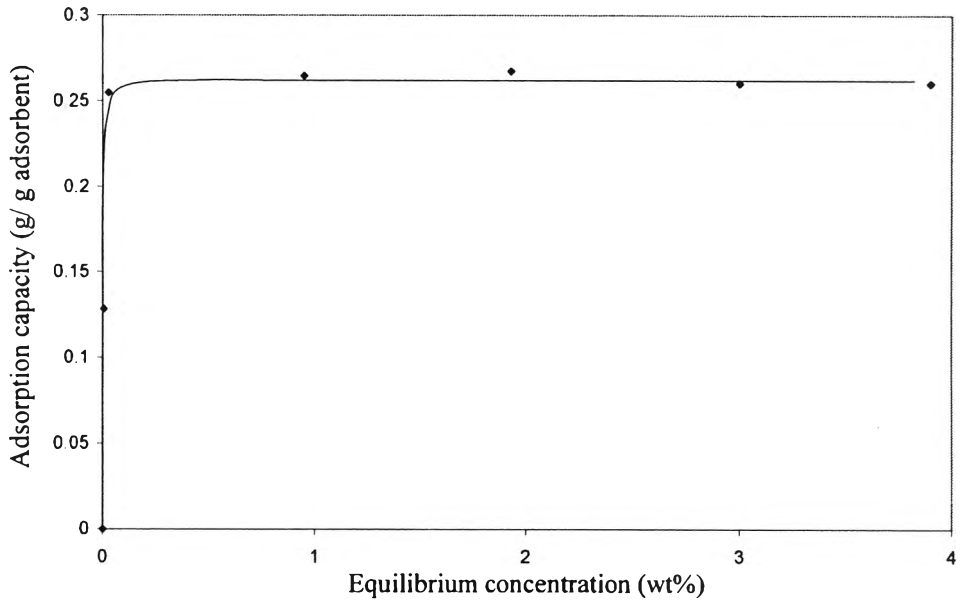

Figure 4.4 Adsorption isotherm of *p*-CNB on CaX at 30°C.

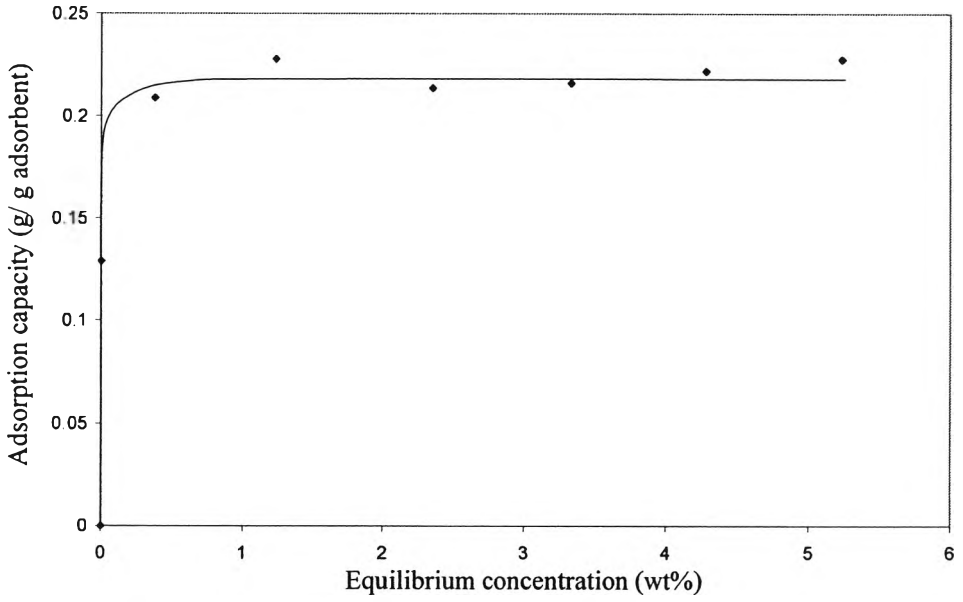

Figure 4.5 Adsorption isotherm of *m*-CNB on SrX at 30°C.

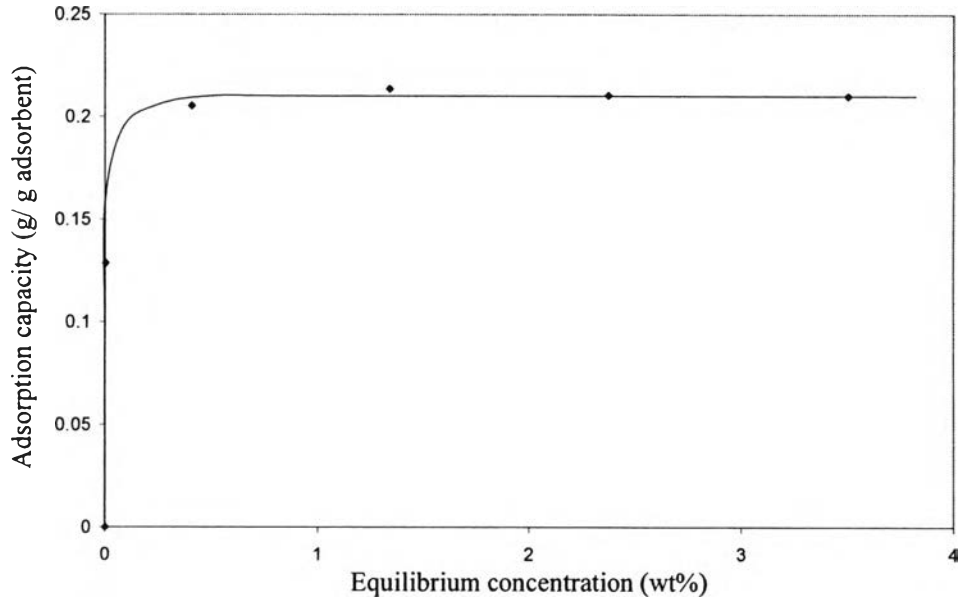

Figure 4.6 Adsorption Isotherm of *p*-CNB on SrX at 30°C.

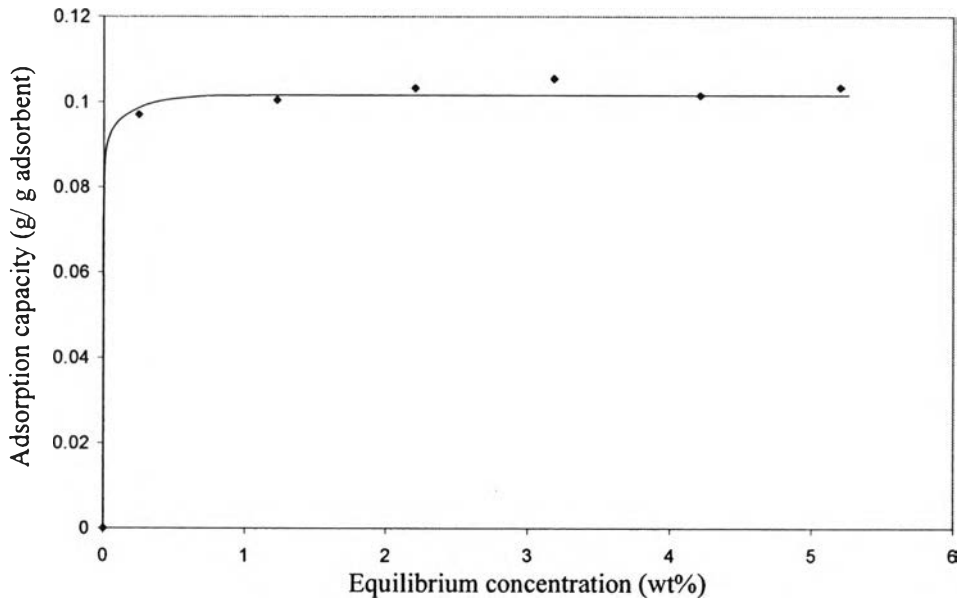

Figure 4.7 Adsorption isotherm of *m*-CNB on BaX at 30°C.

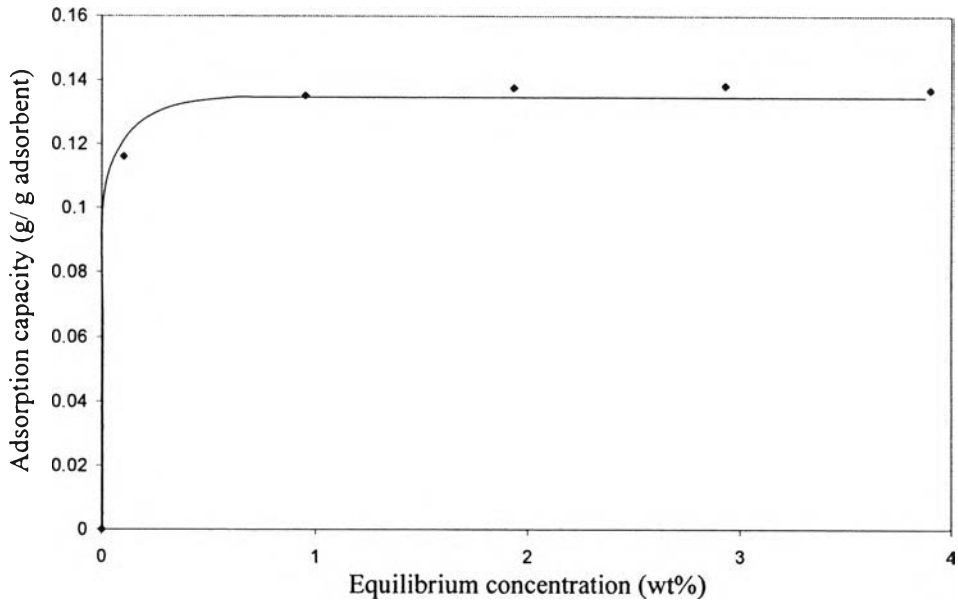

Figure 4.8 Adsorption isotherm of *p*-CNB on BaX at 30°C.

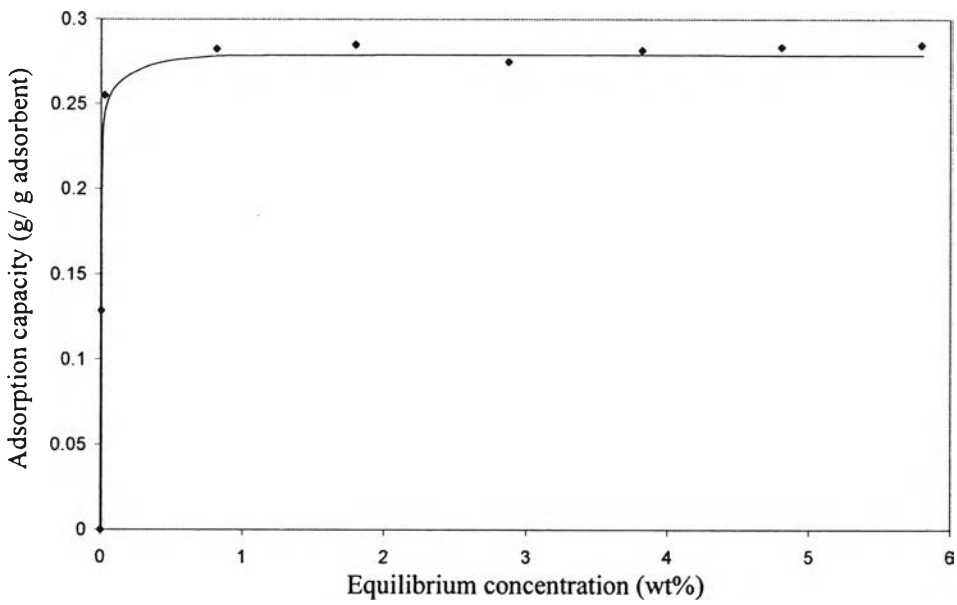

Figure 4.9 Adsorption isotherm of *m*-CNB on MgY at 30°C.

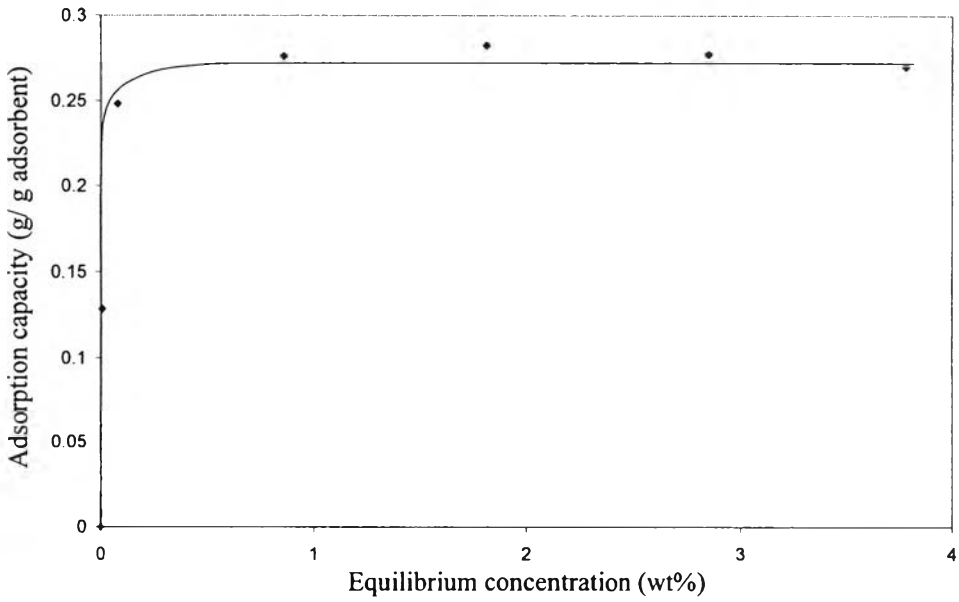

Figure 4.10 Adsorption isotherm of *p*-CNB on MgY at 30°C.

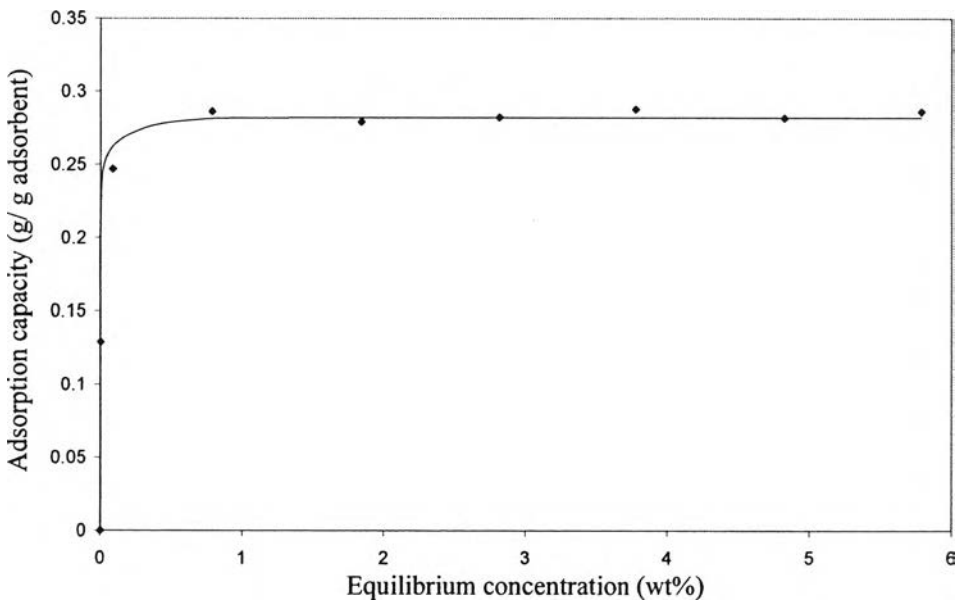

Figure 4.11 Adsorption isotherm of *m*-CNB on CaY at 30°C.

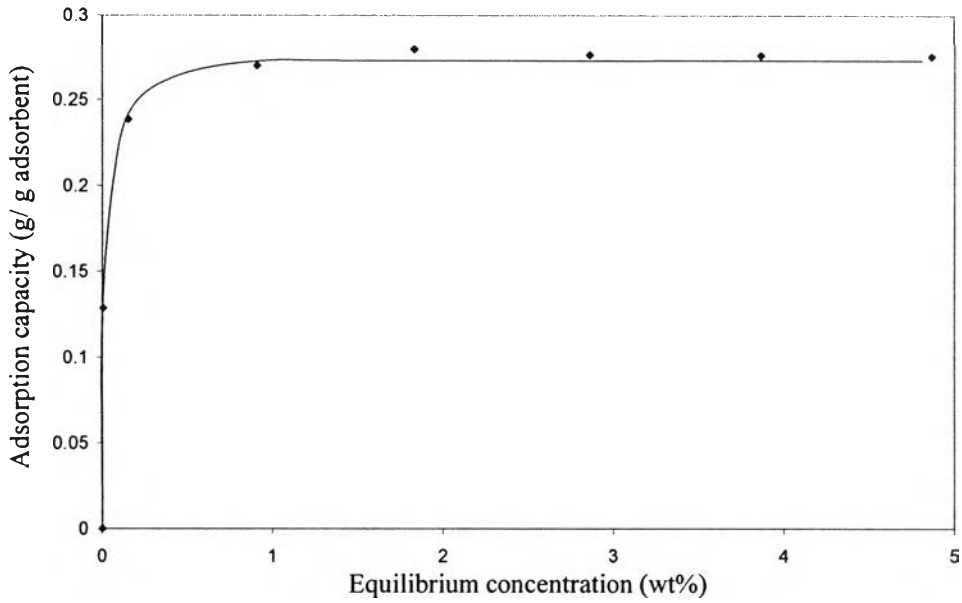

Figure 4.12 Adsorption isotherm of *p*-CNB on CaY at 30°C.

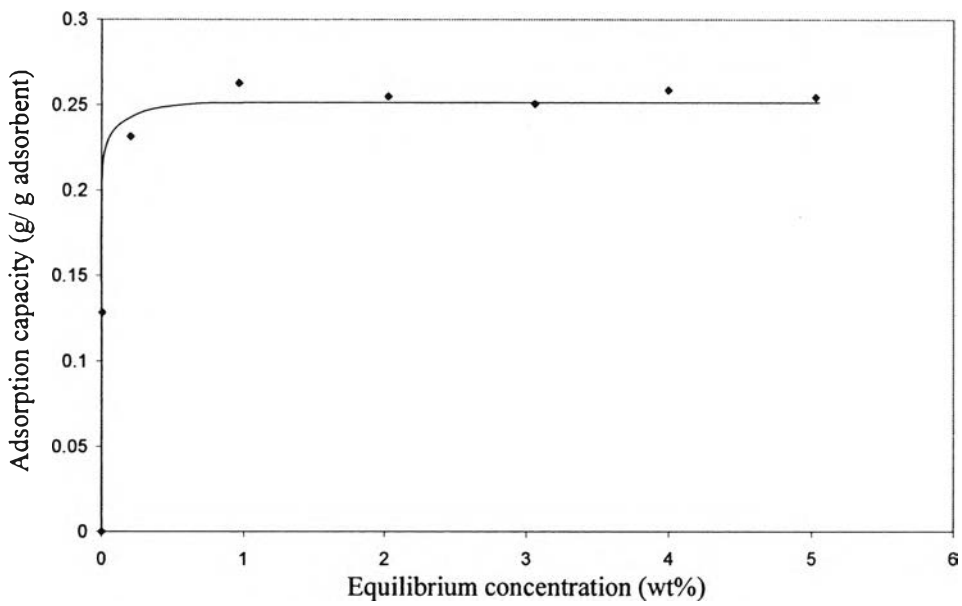

Figure 4.13 Adsorption isotherm of *m*-CNB on SrY at 30°C.

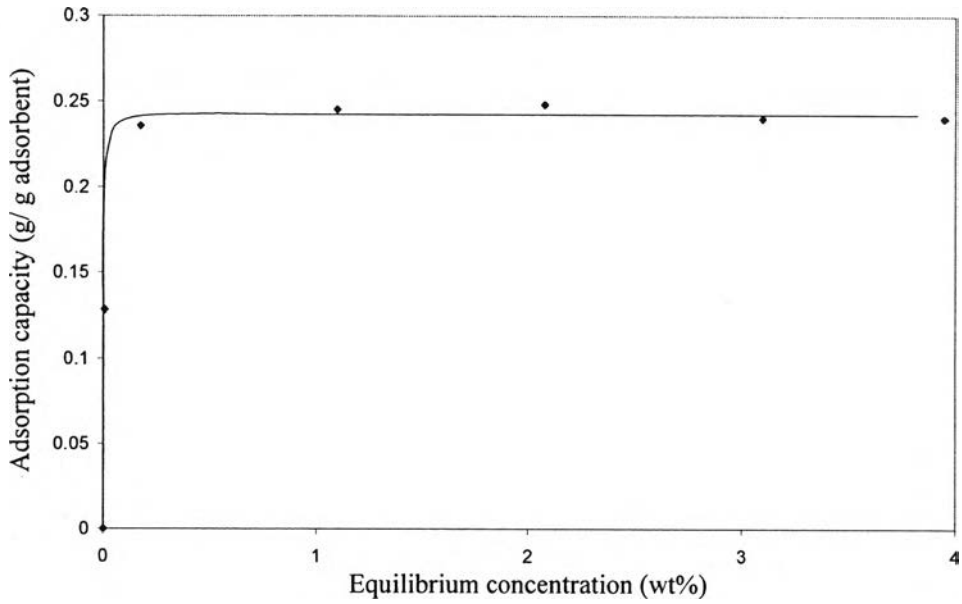

Figure 4.14 Adsorption isotherm of *p*-CNB on SrY at 30°C.

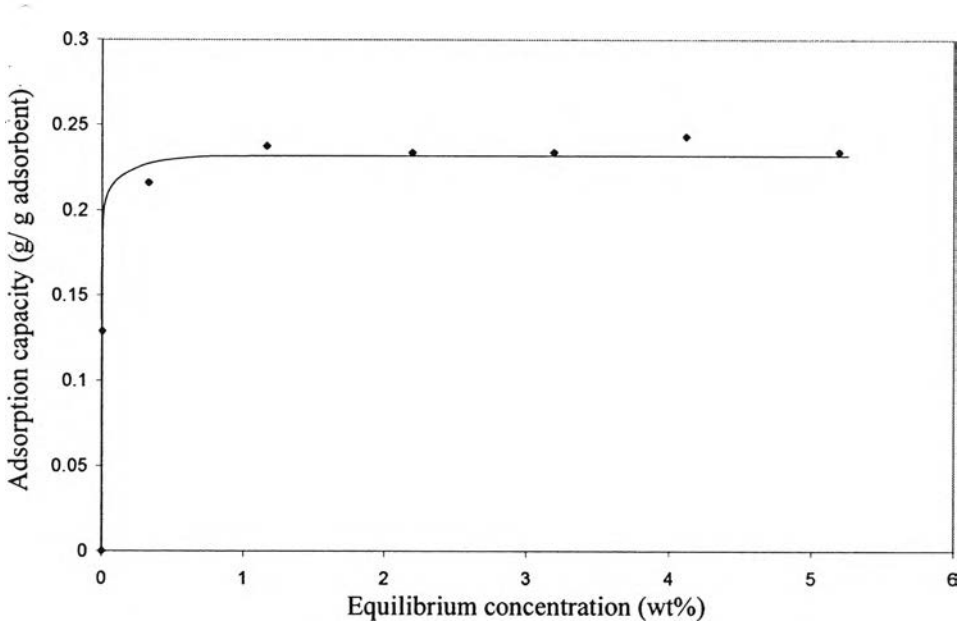

Figure 4.15 Adsorption isotherm of *m*-CNB on BaY at 30°C.

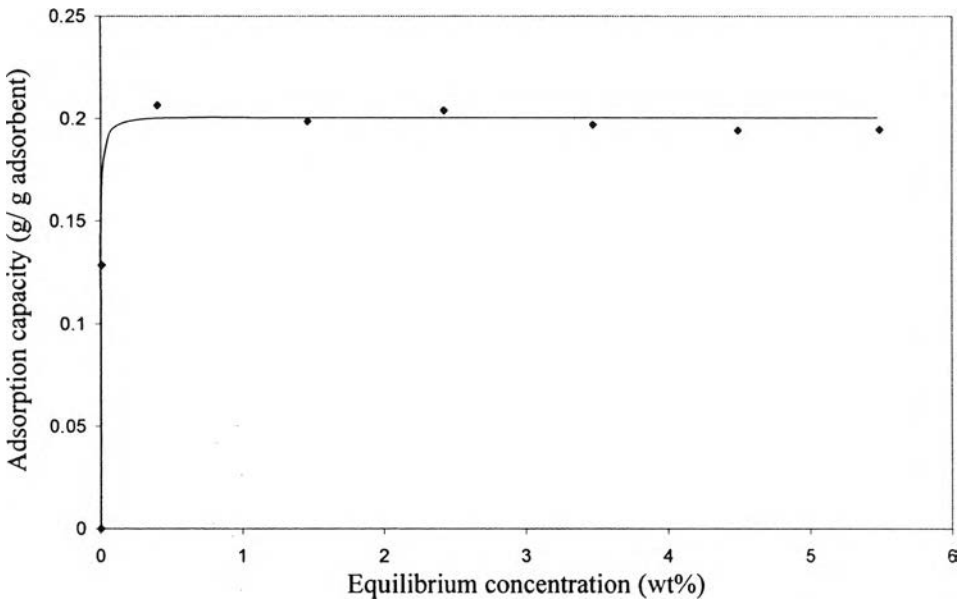

Figure 4.16 Adsorption isotherm of *p*-CNB on BaY at 30°C.

For this experiment, the classical Langmuir model (Eq. (4.1)) was used to fit the experimental data and described the adsorption isotherm.

$$Q = \frac{Q_{max} K C_e}{1 + K C_e}, \tag{4.1}$$

where Q is the equilibrium adsorption capacity in grams of adsorbed component on zeolite per gram of adsorbent, C_e is the equilibrium concentration, Q_{max} is the maximum capacity or saturation capacity, and K is the equilibrium constant (Minceva and Rodrigues, 2004).

The maximum capacity (Q_{max}), equilibrium constant (K), and coefficient of determination (R^2) were determined and reported in Tables A1 and A2. The equation was fitted well with all of the experimental data as the determination coefficient (R^2) is close to unity.

Table 4.1 Adsorption capacities of *m*- and *p*-CNB on FAU zeolite with the alkaline earth exchanged cations

Adsorbent	Ionic radius (Å)*	Sanderson's intermediate electronegativity (S_{int})**	Adsorption Capacity (g/g adsorbent)	
			m-CNB	*p*-CNB
X zeolite				
Mg	0.72	3.705	0.13	0.12
Ca	0.99	3.754	0.27	0.27
Sr	1.12	3.732	0.22	0.21
Ba	1.35	3.657	0.11	0.14
Y zeolite				
Mg	0.72	3.907	0.29	0.28
Ca	0.99	3.890	0.28	0.28
Sr	1.12	3.883	0.25	0.25
Ba	1.35	3.836	0.24	0.20

*, ** Kraikul *et al.*, 2006

Table 4.1 and Figure 4.17 show the adsorption capacities of *m*- and *p*-CNB on the FAU zeolites with the series of alkaline earth exchanged cation. The adsorption capacities of *m*- and *p*-CNB on both X and Y zeolites decrease with increasing in the cation size in Figure 4.17. This is because some adsorption sites are blocked by a large cation. However, MgX, which consists of the smallest cation, gives the lowest adsorption capacities of CNBs among the other X zeolites. Because the acid strength of MgX, 3.705, is lower than that of SrX and CaX, 3.754 and 3.732, respectively and is higher than the acid strength of BaX, 3.657, which their adsorption capacities of both CNBs increase consequently in their acid strength. According to the MgX adsorption, it could be concluded that the single adsorption behavior of *m*- and *p*-CNB on the FAU zeolites does not rely only on the cation size but also the acid strength of the zeolite.

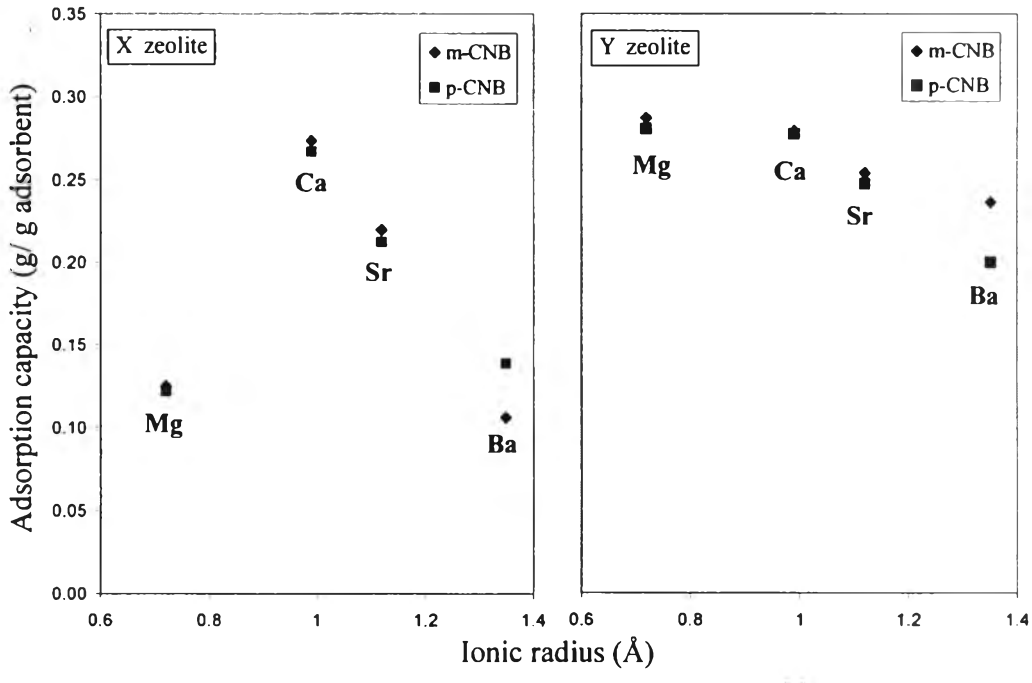

Figure 4.17 Relation of adsorption capacities of *m*- and *p*-CNB on the X and Y zeolites with alkaline earth exchanged cation and ionic radius.

Table 4.2 Kinetic diameters and molecular dipole moments of *m*-CNB and *p*-CNB (Lerdsakulthong, 2007)

CNB isomer	Kinetic diameter (Å)	Molecular dipole moment (D)
m-CNB	5.79	3.73
p-CNB	5.27	2.83

Besides, the difference in molecular dipole moments (μ) of *m*- and *p*-CNB also influences the adsorption capacity. A higher molecular dipole moment results in a higher electron density around molecules or a higher of basicity. From Figure 4.17, the results show that *m*-CNB was preferably adsorbed by the X and Y zeolites more than *p*-CNB except BaX. The Y zeolites adsorb CNBs more than the X zeolites compared with the same exchanged cation because the faujasite zeolites are electron rich framework and *m*-CNB has higher molecular dipole which initiates a strong acid-base interaction (Liu *et al.*, 2007).

As mentioned, the acid strength also has a strong effect on the adsorption performance, which could be varied by the variation of the Si/Al ratio of adsorbent and the exchanging part of exchanged cation (Kulprathipanja *et al.*, 2002). Bigger cation generally is less acidic, which has a higher charge density borne by the oxygen atoms of the framework, leading to the decrease in the interaction between aromatic molecules and adsorbent (Laborde-Boutet *et al.*, 2006). For this experiment, the acid strength of an adsorbent is represented by the Sanderson's intermediate electronegativity (S_{int}), which could be calculated by the following equation.

$$S_{int} = (\prod_i S_i^{n_i})^{1/(\Sigma n_i)}, \tag{4.2}$$

where S_i is the Sanderson's electronegativity of the atom, and n_i is the stoichiometric of the atom in a unit cell of the adsorbent (Dixit and Rao, 1996).

For the ion-exchanged zeolites with a formula of $Na_pM_q(SiO_2)_r(AlO_2)_s$, the S_{int} can be calculated by,

$$S_{int''} = (S_{Na}^{p} S_{M}^{q} S_{Si}^{r} S_{Al}^{s} S_{O}^{2(r+s)})^{1/[p+q+r+s+2(r+s)]} \tag{4.3}$$

The calculated S_{int} of the employed adsorbents are listed in Table 4.1. The highest S_{int} indicates high electron accepting ability and strong adsorbent acid strength (Mortier, 1978; Barthomeuf, 1996).

Generally, the Y zeolites have a S_{int} value higher than the X zeolites or the Y zeolites have higher acid strength than the X zeolites. From Figure 4.18, the results obviously show that the adsorption capacities of CNBs on the Y zeolites are higher than that on the X zeolites compared in the same exchanged cation, meaning that the Y zeolites have stronger adsorption affinity than the X zeolites. The adsorption capacities of *m*- and *p*-CNB increase with the increase in the acid strength of the adsorbents. So, it could be concluded that the adsorption behavior of *m*- and *p*-CNB on the FAU zeolites with di-valence exchanged ion partly depends on an acid-base interaction.

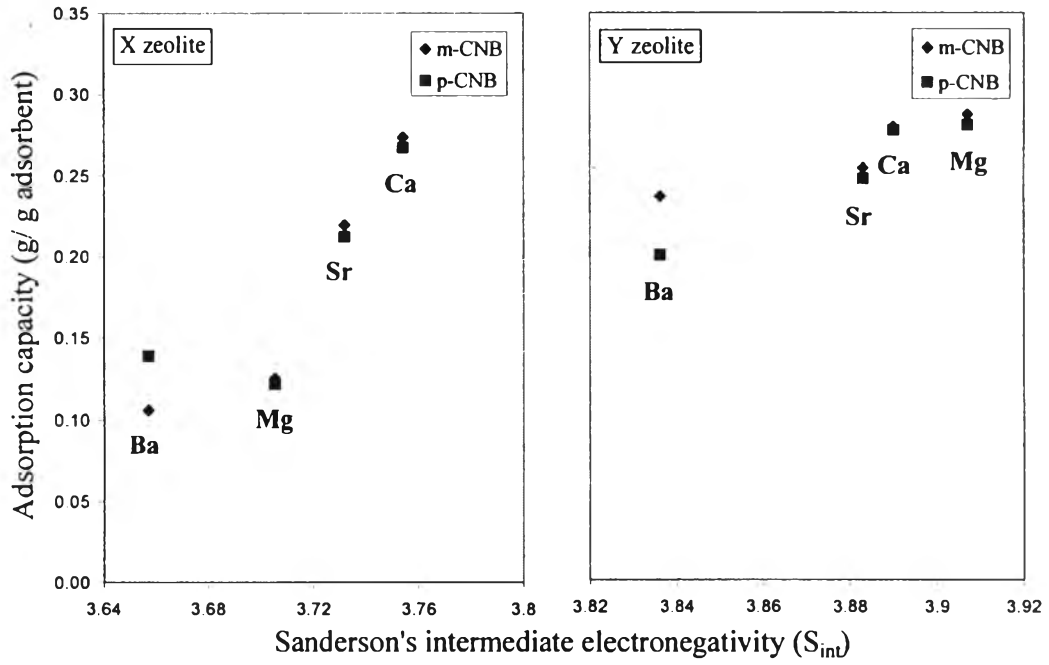

Figure 4.18 Relation of adsorption capacities of *m*- and *p*-CNB on the X and Y zeolites with alkaline earth exchanged cation and Sanderson's intermediate electronegativity (S_{int}).

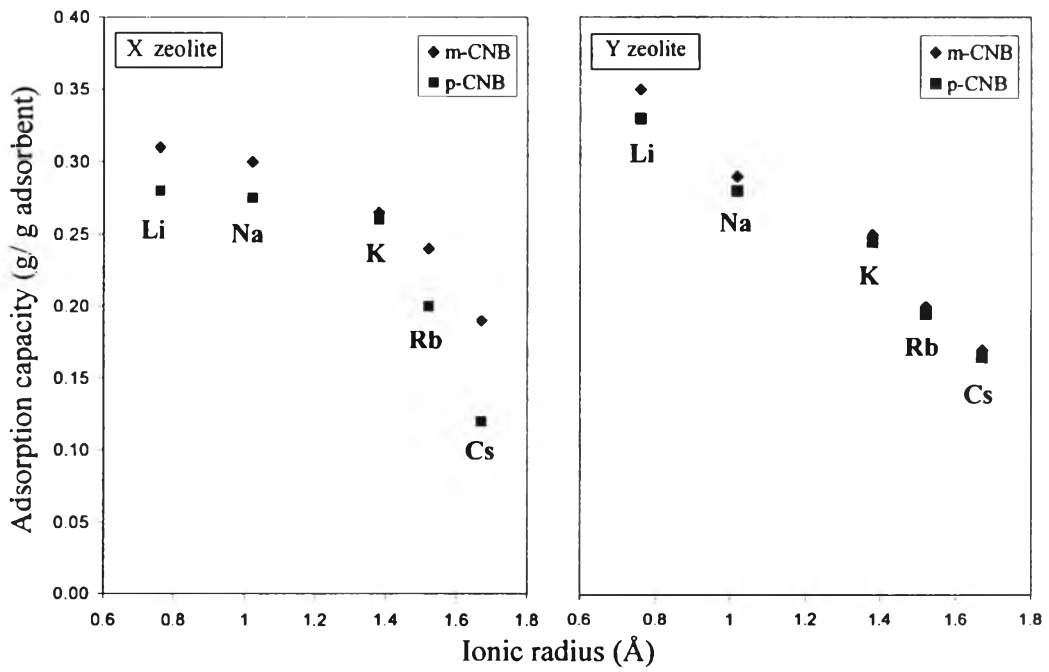

Figure 4.19 Relation of adsorption capacities of *m*- and *p*-CNB on the series of X and Y zeolites with alkaline exchanged cation and ionic radius.

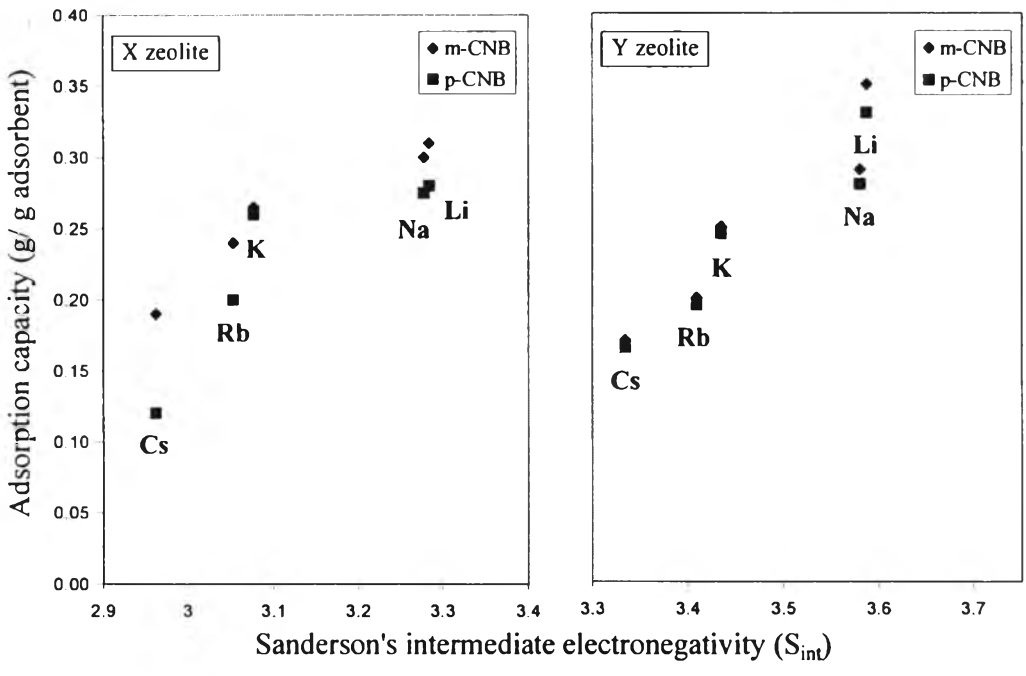

Figure 4.20 Relation of adsorption capacities of *m*- and *p*-CNB on the FAU zeolites with alkaline exchanged cation and Sanderson's intermediate electronegativity (S_{int}).

The adsorption behavior of *m*- and *p*-CNB on the zeolites with alkaline earth exchanged cation is compared with that on the zeolite with alkaline exchanged cation. Figures 4.19 and 4.20 show the relation of the adsorption capacities of CNBs on the zeolite with the alkaline exchanged ion and the ionic radius and the acid strength, respectively. Similar to the zeolites with di-valence exchanged ion, *m*-CNB is selectively adsorbed by the FAU zeolites with mono-valence exchanged ion more than *p*-CNB. The Y zeolites also have higher adsorption capacity than the X zeolites and the adsorption capacities of CNBs increase with an increase in the acid strength of the adsorbent. However, the adsorption behavior of CNBs also depends on the cation size. The capacity d ecreases sequentially with an increase in cation size, which is different from the adsorption behavior of CNBs on the zeolite with the alkaline earth exchanged ions.

4.1.2 Binary Component Adsorption

The adsorption behavior of *m*- and *p*-CNB was also studied in the binary system. The experiments were conducted in the same manner as the previous part except *m*- and *p*-CNB were prepared in the *m*-CNB to *p*-CNB molar ratio of 1:1.

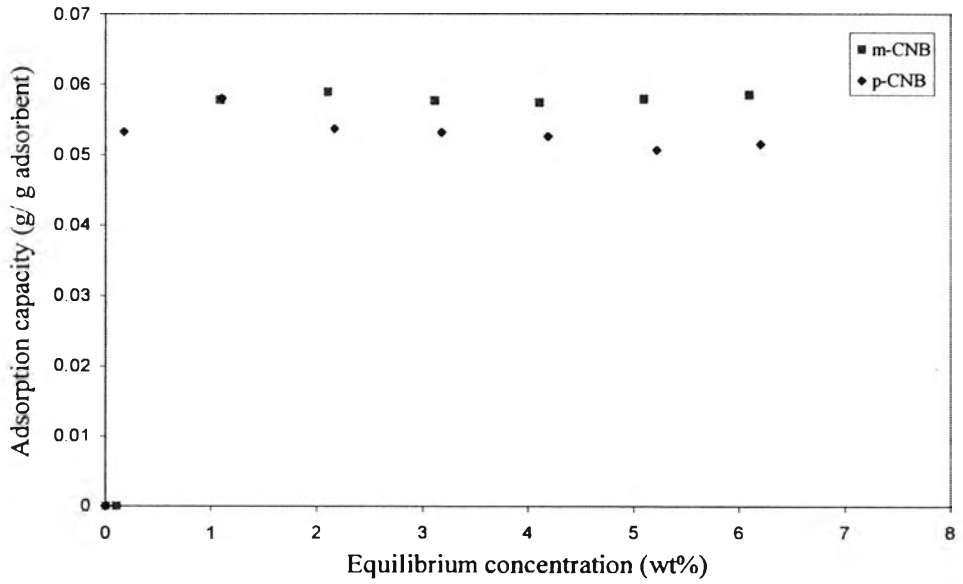

Figure 4.21 Binary adsorption isotherms of *m*- and *p*-CNB on MgX at 30°C.

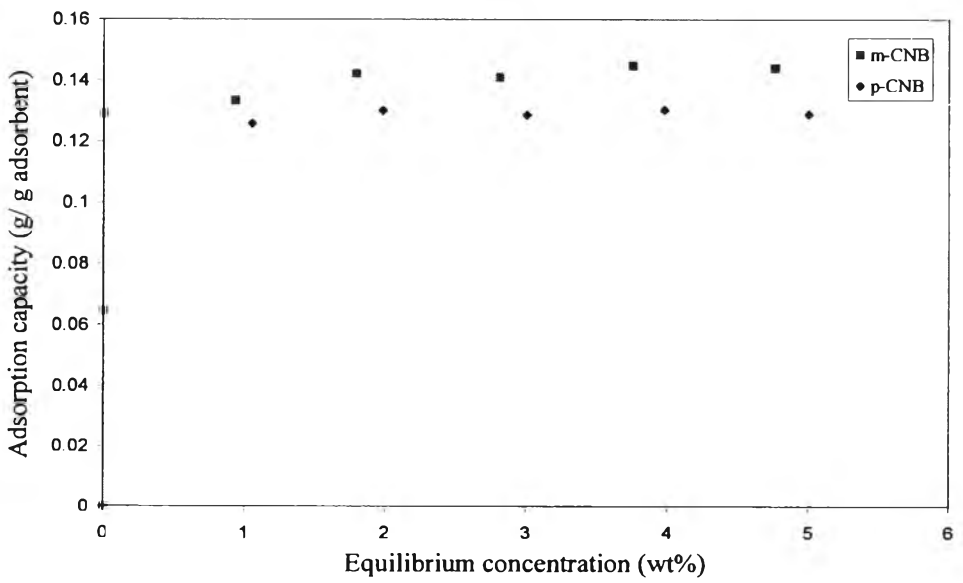

Figure 4.22 Binary adsorption isotherms of *m*- and *p*-CNB on CaX at 30°C.

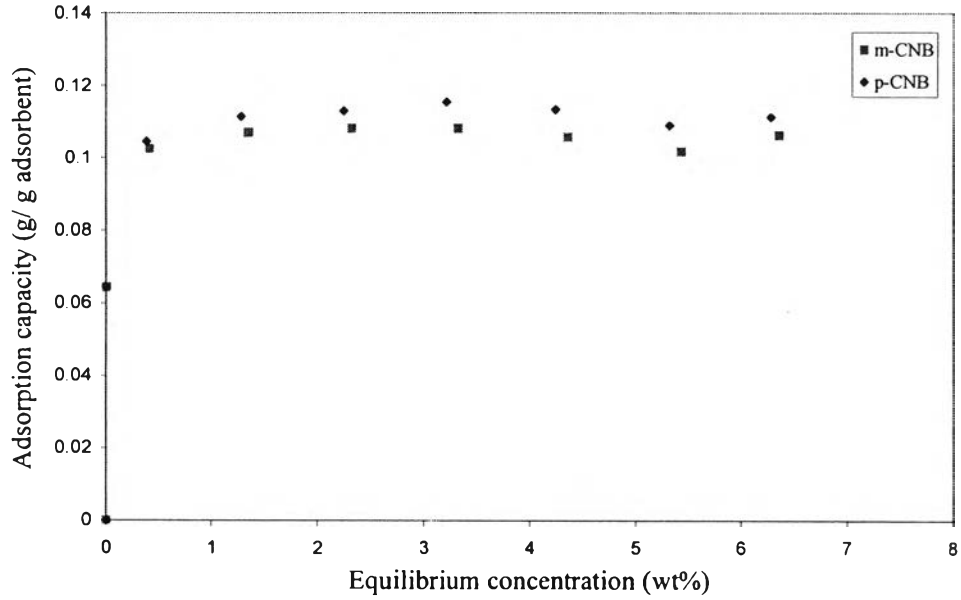

Figure 4.23 Binary adsorption isotherms of *m*- and *p*-CNB on SrX at 30°C.

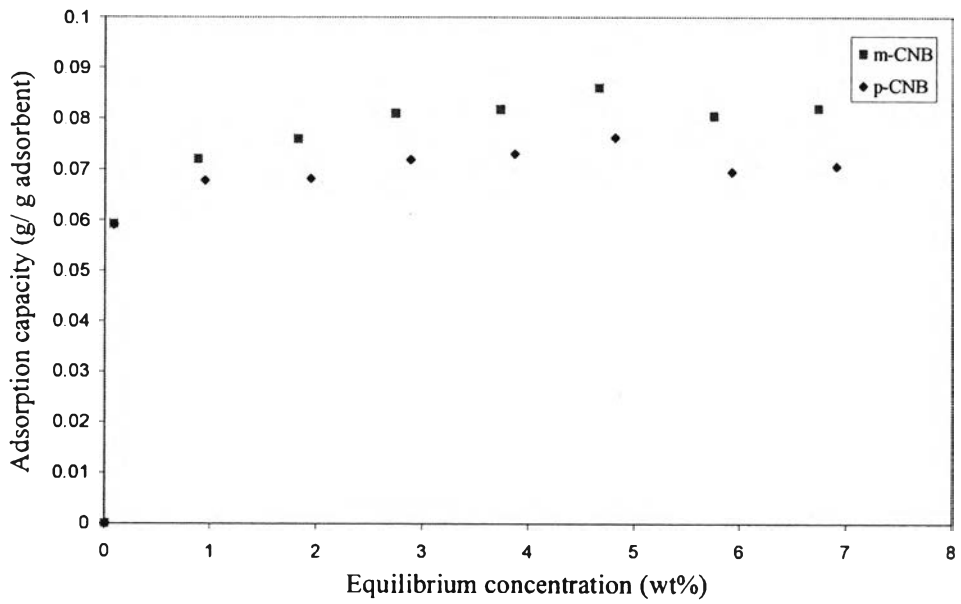

Figure 4.24 Binary adsorption isotherms of *m*- and *p*-CNB on BaX at 30°C.

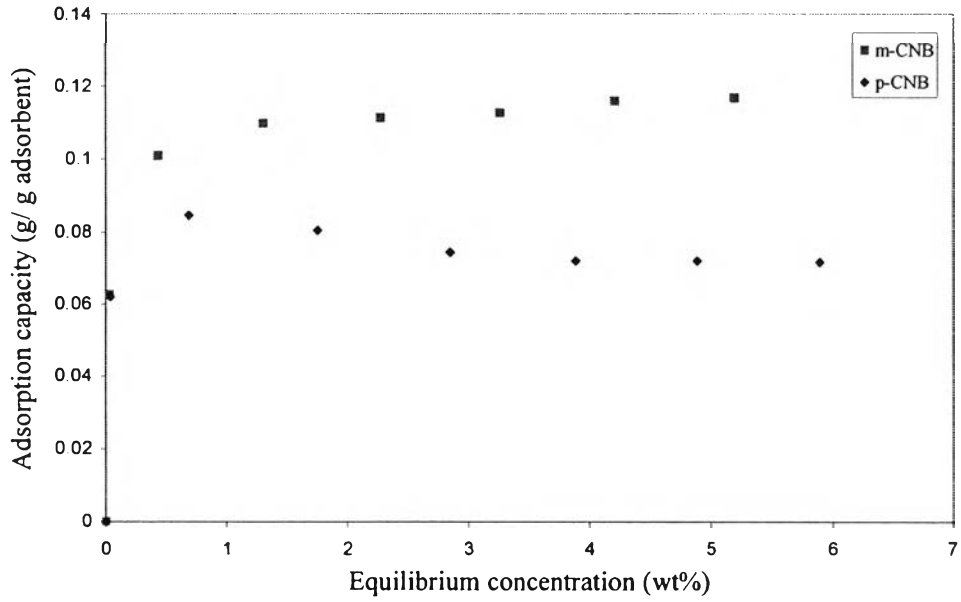

Figure 4.25 Binary adsorption isotherms of *m*- and *p*-CNB on MgY at 30°C.

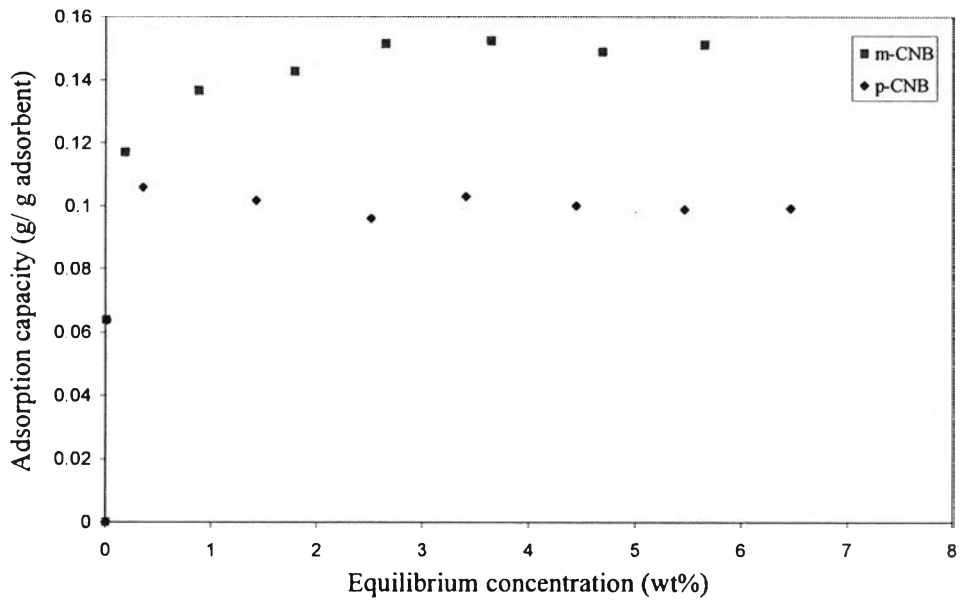

Figure 4.26 Binary adsorption isotherms of *m*- and *p*-CNB on CaY at 30°C.

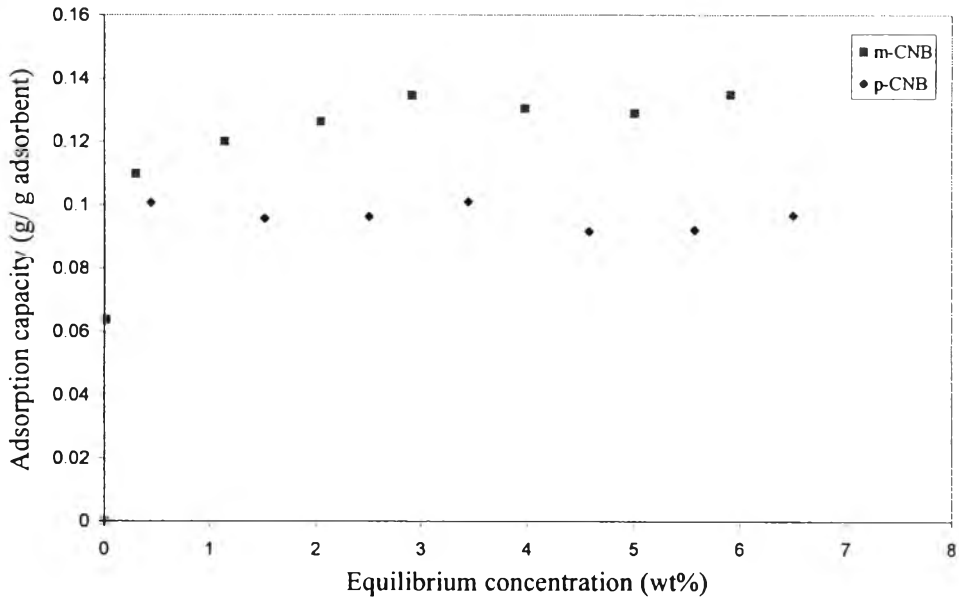

Figure 4.27 Binary adsorption isotherms of *m*- and *p*-CNB on SrY at 30°C.

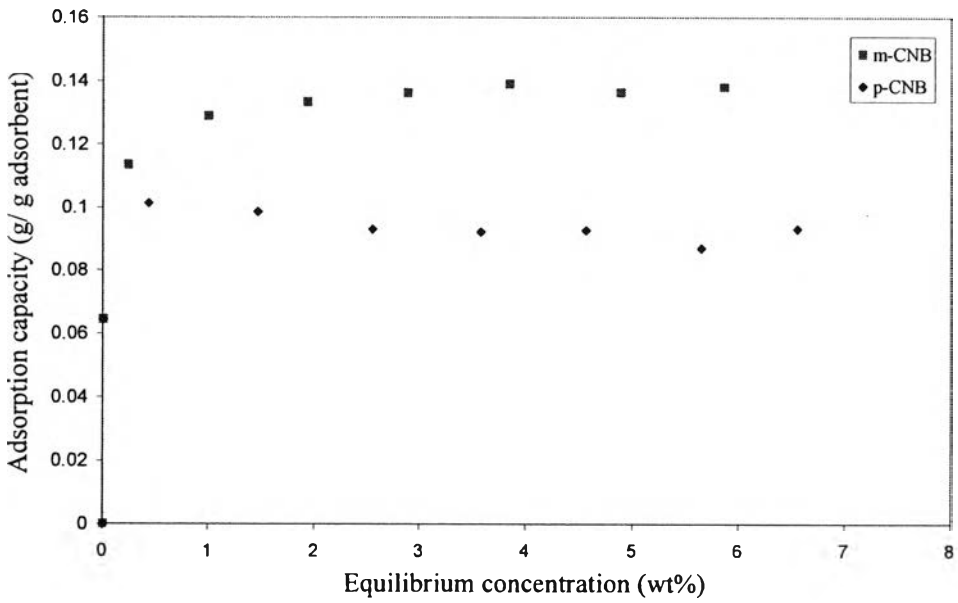

Figure 4.28 Binary adsorption isotherms of *m*- and *p*-CNB on BaY at 30°C.

From Figures 4.21–4.28, the adsorption isotherms of binary system, *m*- and *p*-CNB, on the FAU zeolite are slightly different from the adsorption isotherms of the single system, especially the adsorption isotherm of *p*-CNB. The adsorption capacity of *p*-CNB increases faster than that of *m*-CNB at a low

equilibrium concentration of *m*-CNB and then reaches a lower asymptotic level at a higher equilibrium concentration. It is because of a competitive adsorption between *m*- and *p*-CNB. From Table 4.1, both isomeric CNBs could diffuse through the FAU zeolite easily since their molecular size is smaller than the zeolite pore size. Thus, the molecular diffusion is not a factor that could control this competition. The main reason of this behavior may rely on the acid–base interaction between the zeolites and the isomeric substances, which is similar to the adsorption behavior in the previous part. The zeolites generally adsorb *m*-CNB more than *p*-CNB, especially the Y zeolites. The Y zeolites adsorb *m*-CNB much more than *p*-CNB as shown in Figures 4.25–4.28 because a higher electron density of *m*-CNB and a higher acidity of the zeolites resulting in a stronger electrostatic field interaction. However, SrX does not show the same trend as the others. It slightly favors to adsorb *p*-CNB more than *m*-CNB.

Even though the individual adsorption isotherms of *m*- and *p*-CNB in the binary system are slightly different from those of *m*- and *p*-CNB in the single adsorption, the total adsorption isotherms of both CNBs could be described by the Langmuir model. The total adsorption capacities of both substances on the zeolites are obtained from the summation of the individual adsorption capacities of *m*- and *p*-CNB at the same equilibrium concentration as shown in Figures 4.29 and 4.30.

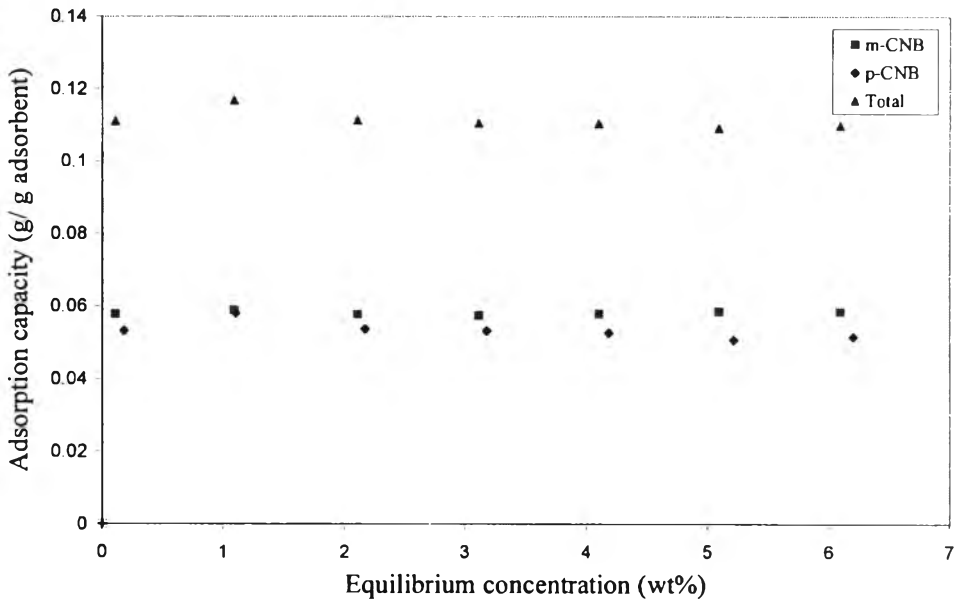

Figure 4.29 Binary competitive adsorption and total adsorption capacity isotherms at 30°C on MgX.

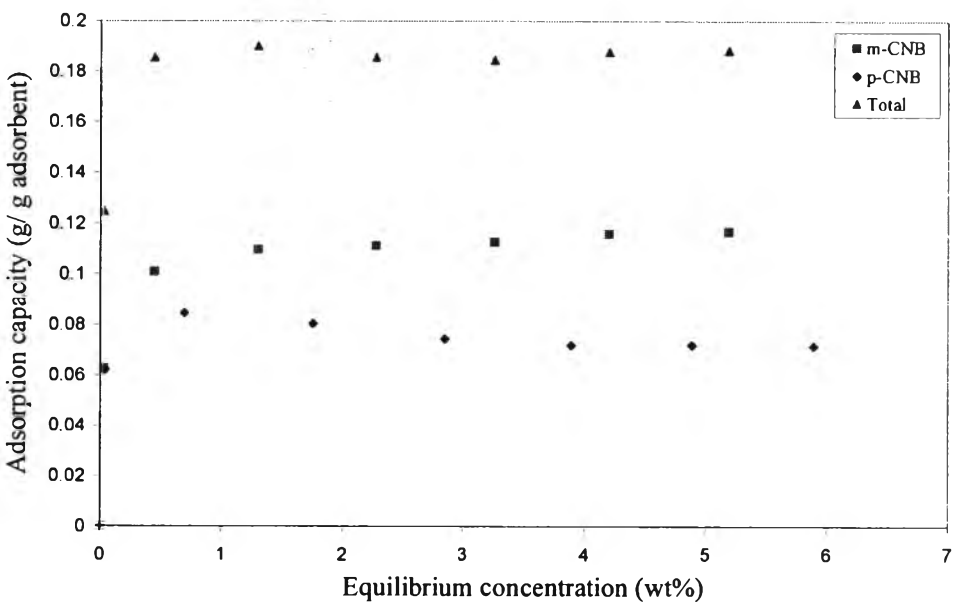

Figure 4.30 Binary competitive adsorption and total adsorption capacity isotherms at 30°C on MgY.

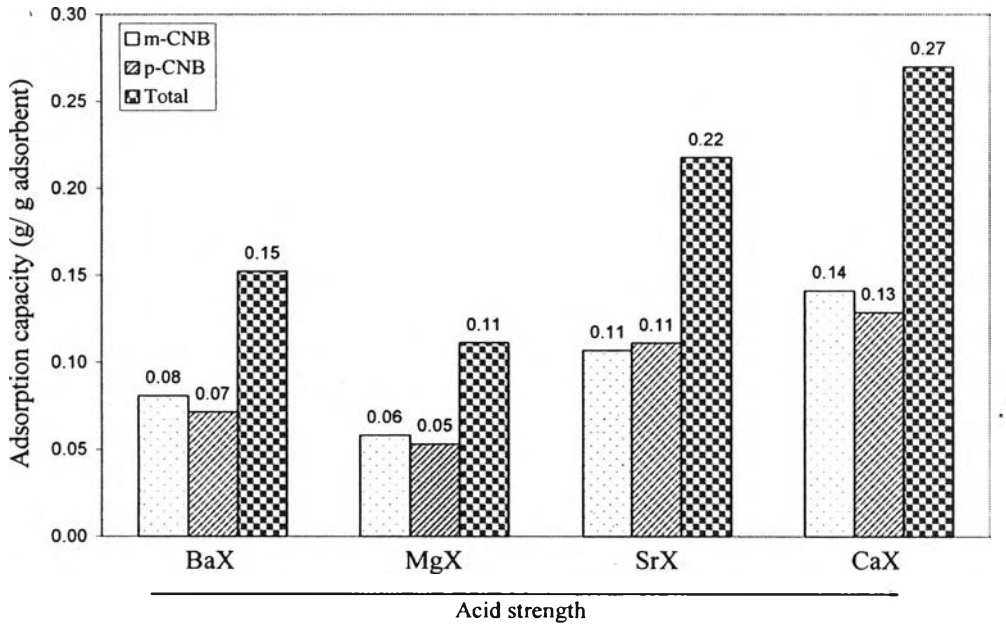

Figure 4.31 Adsorption capacities of *m*- and *p*-CNB, and total adsorption capacity for the binary competitive adsorption with acid strength of the X zeolites with alkaline earth exchanged cation.

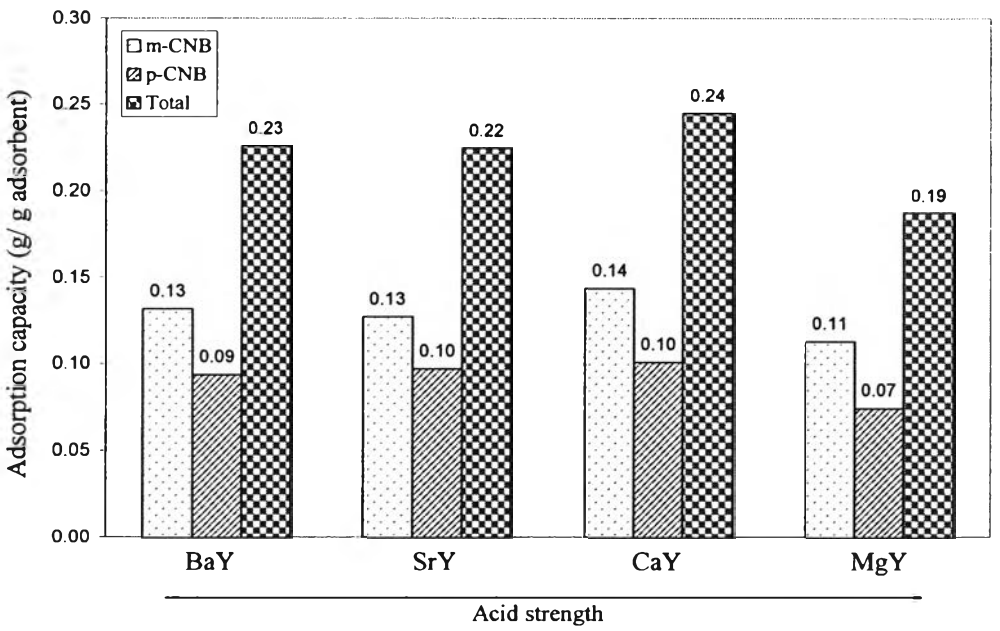

Figure 4.32 Adsorption capacities of *m*- and *p*-CNB, and total adsorption capacity for the binary competitive adsorption with acid strength of theY zeolites with alkaline earth exchanged cation.

Figures 4.31–4.34 show the adsorption capacities of *m*- and *p*-CNB, and the total adsorption capacity on the zeolites cooperated with the mono-valence and di-valence exchanged cations. The acid strength of the adsorbent plays an important role on the adsorption capacities of both CNBs and the total adsorption capacity on both zeolites. The adsorption capacities of *m*-CNB and *p*-CNB, and the total adsorption capacities increase with an increase in acid strength of the adsorbent except MgX, and MgY. It may because of the effect of competitive adsorption of *m*- and *p*-CNB.

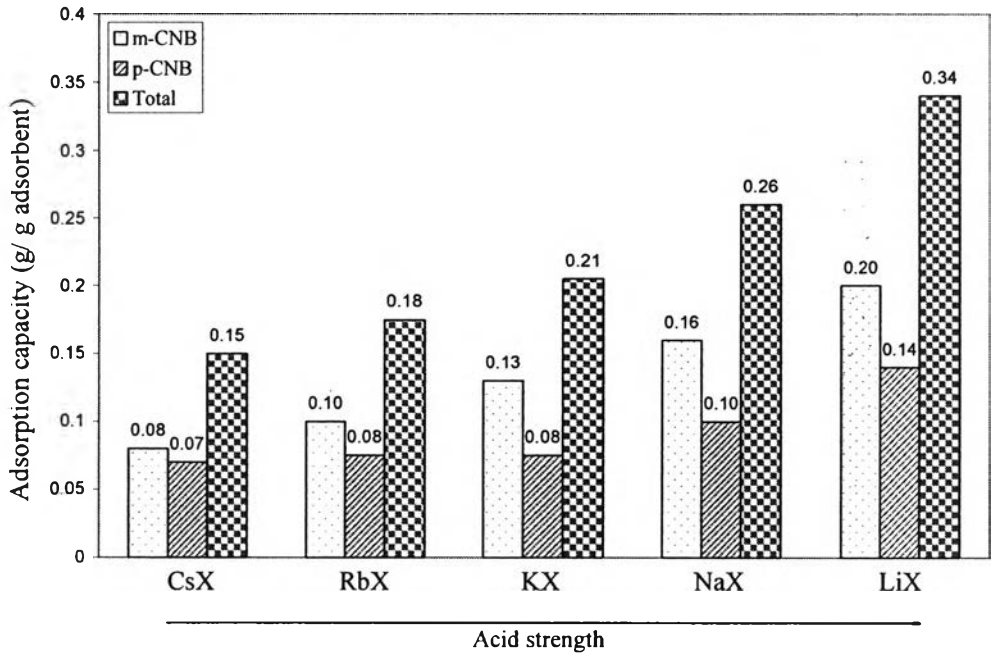

Figure 4.33 Adsorption capacities of *m*- and *p*-CNB, and total adsorption capacity for the binary competitive adsorption with acid strength of the X zeolites with alkaline exchanged cation.

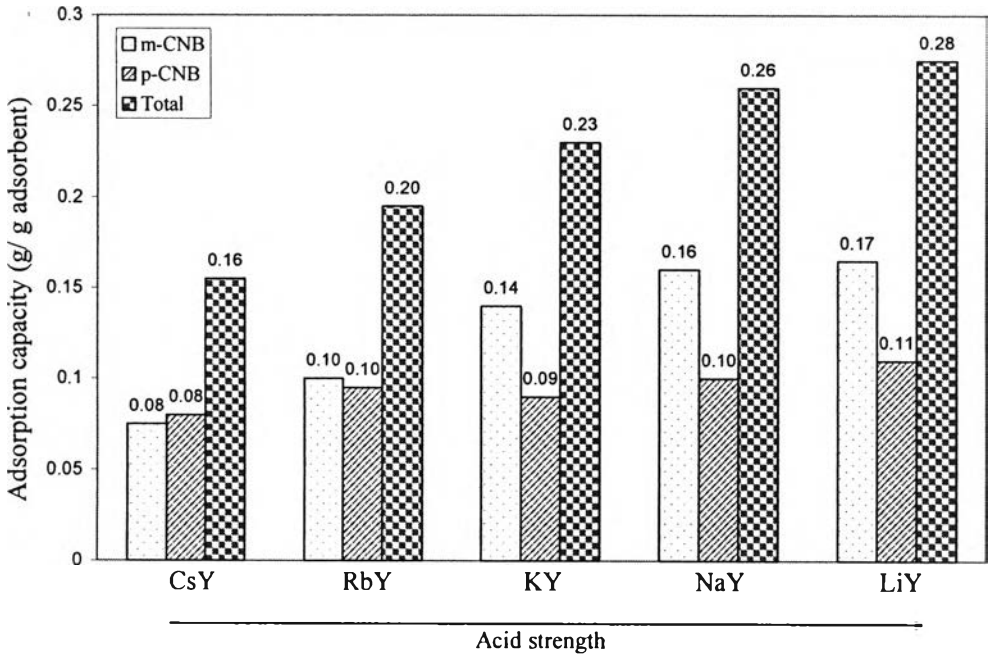

Figure 4.34 Adsorption capacities of *m*- and *p*-CNB, and total adsorption capacity for the binary competitive adsorption with acid strength of the Y zeolites with alkaline exchanged cation.

Nevertheless, this study also reports the adsorption *m*-/ *p*-CNB selectivity of the zeolites. It was calculated from Equation 2.5:

$$\alpha_{AB} = \frac{X_A / X_B}{Y_A / Y_B} \tag{2.5}$$

where X_A and Y_A are, respectively, the mole fractions of component A in adsorbed and fluid phases at equilibrium. For this study, A and B were represented by *m*-CNB and *p*-CNB, respectively.

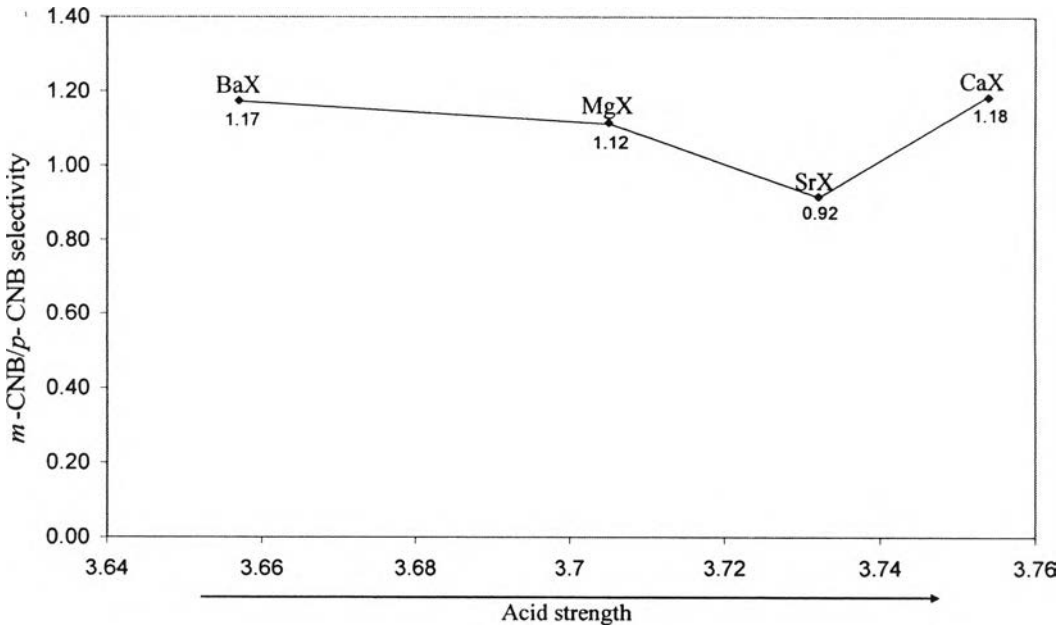

Figure 4.35 *m*-CNB/ *p*-CNB adsorption selectivity of the X zeolites with alkaline earth exchanged cation as function of Sanderson's intermediate electronegativity (S_{int}).

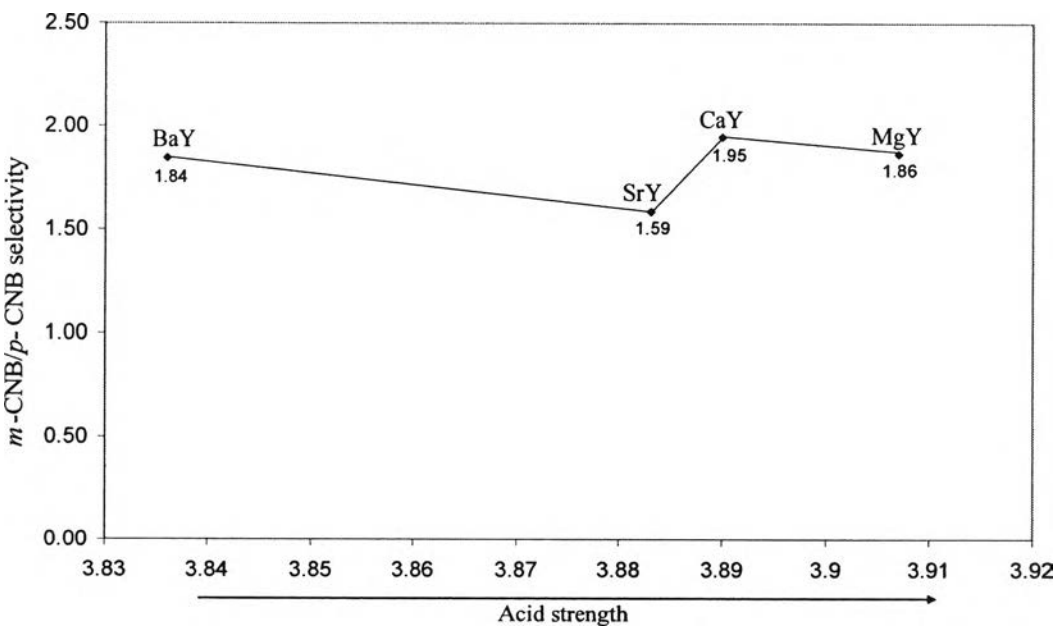

Figure 4.36 *m*-CNB/ *p*-CNB adsorption selectivity of the Y zeolites with alkaline earth exchanged cation as function of Sanderson's intermediate electronegativity (S_{int}).

Generally, most of the employed adsorbents preferably adsorb *m*-CNB more than *p*-CNB due to a higher basicity. But for SrX, it selectively adsorbs *p*-CNB more than *m*-CNB as shown by the selectivity less than unity. The Y zeolites, which have a higher acid strength, give a higher *m*-/*p*-CNB adsorption selectivity than the X zeolites with the di-valence exchanged ion (Figures 4.35 and 4.36). The Sanderson's intermediate electronegativity of the adsorbents (S_{int}) was calculated as a representative to the acid strength of the adsorbent. The higher S_{int} indicates high electron accepting ability and strong adsorbent acid strength (Kraikul *et al.*, 2006). CaY gives the highest selectivity, followed by MgY, BaY, and SrY gives the lowest selectivity. However, the acid strength does not affect greatly on the selectivity because the selectivity does not increase much with the increase in the acid strength of both X and Y zeolites with different exchanged cations.

Comparison between the selectivity of the zeolite with mono-valence and di-valence exchanged ion shows that there are a few differences. Firstly, the trend of the selectivity of the zeolite is considered. The selectivity of the zeolite with alkaline earth cation corresponds with the classical Langmuir model due to the constant of the selectivity value at any equilibrium concentration, which shows an ideal adsorption behavior (Titus *et al.*, 2003). Meanwhile, the adsorption selectivity of the zeolite with mono-valence exchanged ion shows a non-ideal behavior. The selectivity depends on the composition in the fluid phase. It decreases with the increase in the *m*-CNB equilibrium concentration in Figure 4.37.

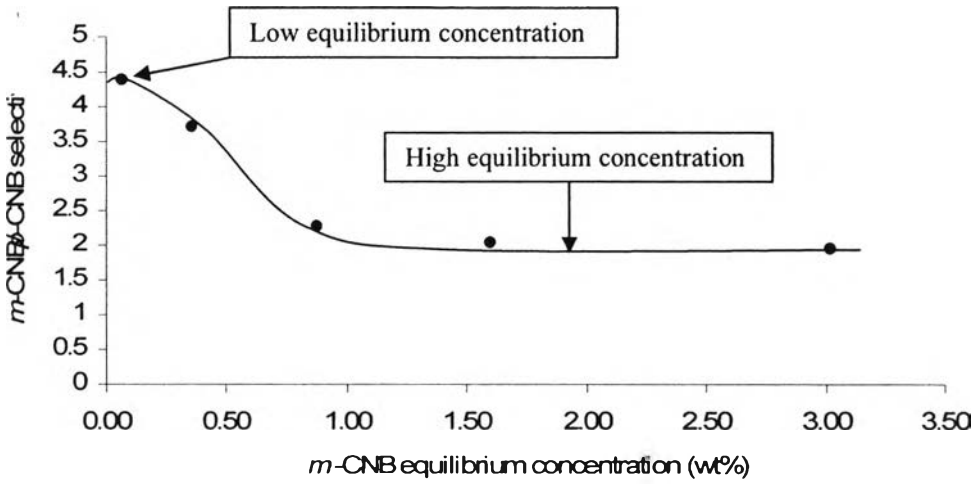

Figure 4.37 *m*-CNB/ *p*-CNB selectivity as a function of equilibrium concentration in liquid phase on NaY zeolite (Lerdsakulthong, 2007).

Moreover, the selectivity of the zeolites with alkaline exchanged cation relies significantly on the acid strength of the adsorbent. NaY is the most appropriate adsorbent among the employed zeolites with alkaline ion exchange as shown in Figure 4.38 (Lerdsakulthong, 2007). For the zeolites with alkaline earth exchanged ion, CaY is the most proper adsorbent because it gives the highest the adsorption capacity of *m*-CNB and the highest *m*-CNB/*p*-CNB selectivity. If NaY is compared with CaY, at a low equilibrium concentration of *m*-CNB, NaY gives a better performance than CaY because NaY could adsorb *m*-CNB more than CaY and NaY has the *m*-/ *p*-CNB selectivity almost twin higher than CaY. But at a high equilibrium concentration, the adsorption selectivities of both NaY and CaY are comparable.

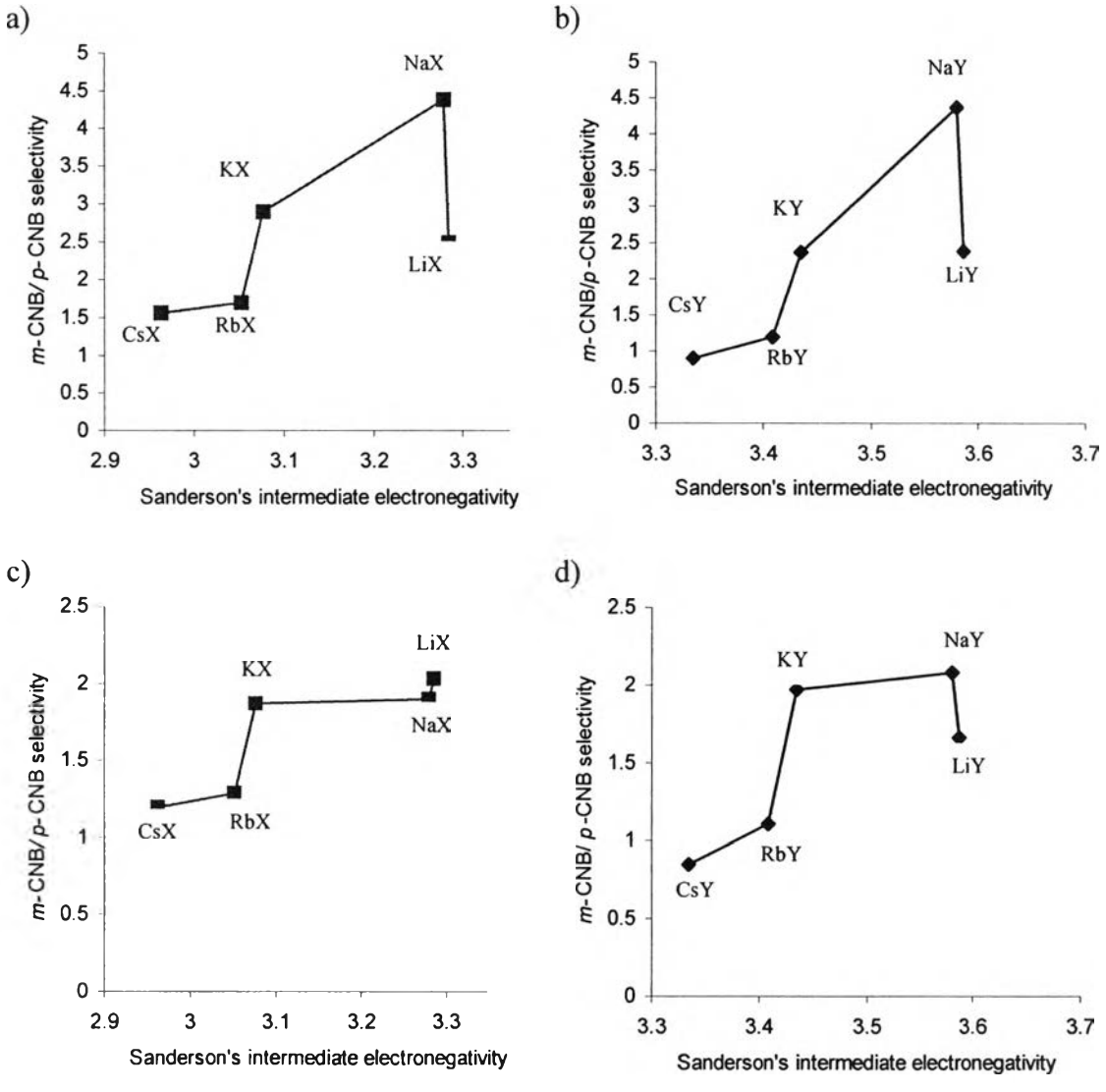

Figure 4.38 *m*-CNB/ *p*-CNB selectivity of the zeolites with alkaline exchanged cation at low (a and b) and high (c and d) equilibrium concentration as a function of Sanderson's intermediate electronegativity (S_{int}) (Lerdsakulthong, 2007).

4.2 Effect of FAU Zeolite on the Crystallization of *m*- and *p*-CNB

4.2.1 Effect of FAU Zeolites on CNBs Mixture Composition

According to UOP research work, only a few grains of zeolite could deviate the precipitate composition of binary *m*- and *p*-CNB system at the eutectic temperature, ≈22°C, was mentioned. For this experiment, 7 g of CNBs mixture with 65 wt% *m*-CNB and 35 wt% *p*-CNB was prepared in a homogeneous phase at 30°C. NaX, CaX, NaY, and CaY were calcined at 350°C for an hour prior to the experiment and added, 10 grains or ≈0.0014 g, individually into the mixture at the center of the crystallization unit. The mixture was stirred to accelerate the system approaches to equilibrium. Then, the mixture was measured for its composition after adding the zeolite. However, the compositions of the mixture before and after adding the zeolite are still similar, which implies that the presence of the zeolites hardly affects the *m*- and *p*-CNB compositions in the mixture.

Table 4.3 *m*- and *p*-CNB composition in the original mixture and the mixture with 10 grains of the zeolites at 30°C

Liquid mixture	Composition (%)	
	***m*-CNB**	***p*-CNB**
Without zeolite	65.00	35.00
With 10 grains of NaX	64.98	35.02
With 10 grains of CaX	64.98	35.02
With 10 grains of NaY	64.98	35.02
With 10 grains of CaY	64.97	35.03

4.2.2 Effect of FAU Zeolites on the Precipitate Composition of *m*- and *p*-CNB

For this experiment, the mixture is started at the composition of 65 wt% *m*-CNB and 35 wt% *p*-CNB. In the condition without zeolite, almost pure precipitates of *m*-CNB generated gradually at 96 wt% *m*-CNB and 4 wt% *p*-CNB,

when the system temperature was decreased and held at 22°C, the eutectic temperature of binary *m*- and *p*-CNB system as shown in the phase diagram of *m*- and *p*-CNB (Figure 4.39).

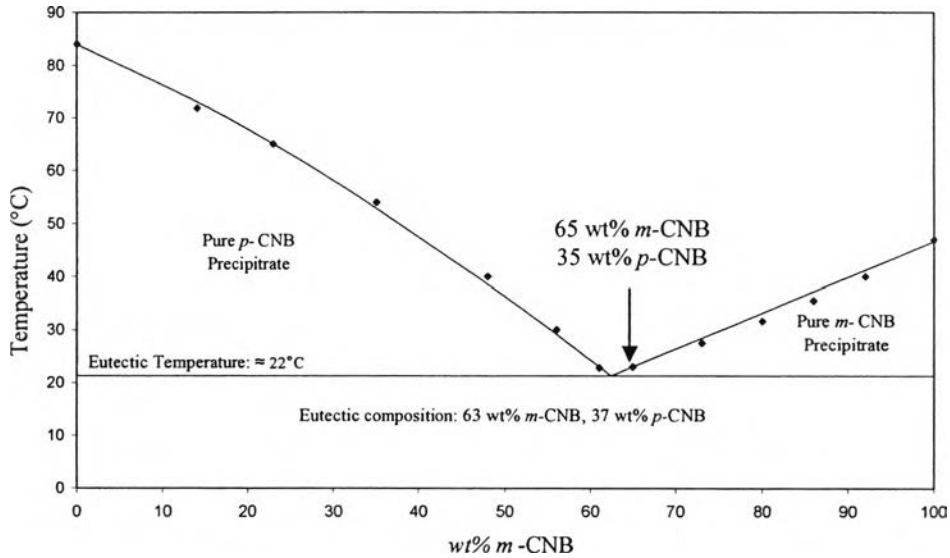

Figure 4.39 Binary phase diagram of *m*-CNB and *p*-CNB (Sulzer Chemtech Pte., Ltd).

On the other hand, the mixture of CNBs with 10 grains of a FAU zeolite was cooled to 22°C. The precipitates and the mother liquor were taken for CNBs composition (run#1) analysis. Afterwards, the experiment was repeated by heating the mixture back to the homogeneous phase. The mixture was then cooled to the eutectic temperature in order to ensure that the result was reproducible even the zeolite was saturated. The CNBs composition (run#2) was analyzed. Normally, the CNBs precipitates initiate throughout the crystallizer. Thus, the precipitates were taken for the analysis in two locations; the precipitate located near the zeolite or area (a) and the precipitate located far from the zeolite or area (b) in Figure 4.40. The CNBs compositions of the precipitates in both positions are shown in Tables 4.4 and 4.5, respectively.

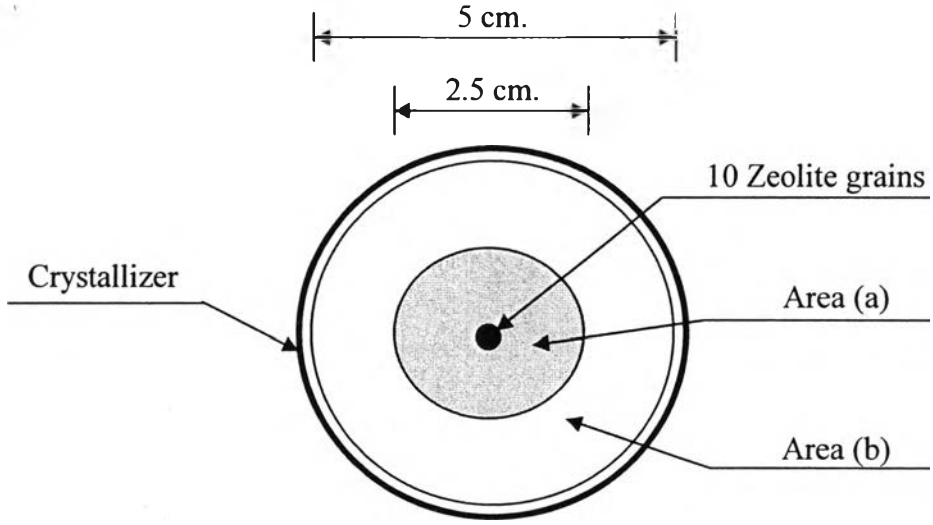

Figure 4.40 Locations where precipitates are taken for *m*- and *p*-CNB composition analysis.

Table 4.4 Composition of *m*- and *p*-CNB in the precipitates located near the zeolite or area (a) at 22°C

Zeolite	Run# 1			Run# 2		
	Composition (%)		%	Composition (%)		%
	m-CNB	*p*-CNB	difference*	*m*-CNB	*p*-CNB	difference*
NaX	8.75	91.25	56.25	9.66	90.34	55.34
CaX	15.54	85.46	49.46	14.23	85.77	50.77
NaY	8.05	91.95	56.95	6.33	93.67	58.67
CaY	13.55	86.45	51.45	13.32	86.68	51.68

*% difference is the different percentage of *m*-CNB composition between precipitate and starting mixture, 65 wt% *m*-CNB.

Table 4.5 Composition of *m*- and *p*-CNB in the precipitates located far from the zeolite or area (b) at 22°C

Zeolite	Run# 1			Run# 2		
	Composition (%)		% difference*	Composition (%)		% difference*
	m-CNB	*p*-CNB		*m*-CNB	*p*-CNB	
NaX	20.05	79.95	44.95	36.23	63.77	28.77
CaX	25.43	74.57	39.57	40.15	59.85	24.85
NaY	26.47	73.53	38.53	43.11	56.89	21.89
CaY	30.40	69.60	34.60	35.09	64.91	29.91

*% difference is the different percentage of *m*-CNB composition between precipitate and starting mixture, 65 wt% *m*-CNB.

From Tables 4.4 and 4.5, the composition of CNBs in the precipitates at both positions appears to be rich in *p*-CNB, which is opposite from the result of the condition without zeolite, especially the precipitates near the zeolite (area (a)). From Table 4.4, the results show the addition of the zeolites with the alkaline exchanged cations resulted in higher composition of *p*-CNB in the precipitates than the zeolites with the alkaline earth exchanged cations for both zeolites. The Y zeolites give a slightly higher of *p*-CNB composition than the X zeolites. In Table 4.5, the alkaline exchanged cations also offer the higher composition of *p*-CNB than the alkaline earth exchanged cations, except NaY. The composition of *p*-CNB in the precipitates in the area (b) is lower than that in the area (a) for all types of zeolite because there are agglomerations of the precipitates in the area (b).

From the results, the presence of the zeolite makes the precipitates changed from rich in *m*-CNB to rich in *p*-CNB. It may be because of the formation of the composition gradient in the mixture around the zeolite while the temperature was being decreased. The CNBs compositions of the mixture can be observed between the two locations, the mixture at the zeolite or area (a), and at the area far from the zeolite or area (b) at 30°C and 22°C as shown in Figure 4.40.

Table 4.6 Composition of *m*- and *p*-CNB in the mixture at the zeolite or area (a) and far from the zeolite or area (b) at 30 and 22°C

Zeolite	Temperature (°C)	(a) area		(b) area	
		Composition (%)		Composition (%)	
		m-CNB	*p*-CNB	*m*-CNB	*p*-CNB
NaX	30°C	64.98	35.02	64.98	35.02
	22°C	64.99	35.01	64.99	35.01
CaX	30°C	64.98	35.02	64.97	35.03
	22°C	64.98	35.02	64.97	35.03
NaY	30°C	64.98	35.02	64.98	35.02
	22°C	64.98	35.02	64.99	35.01
CaY	30°C	64.97	35.03	64.97	35.03
	22°C	64.99	35.01	64.98	35.02

Table 4.6 shows the CNBs compositions of the two locations at 30°C, starting temperature, 22°C, precipitating temperature. The data show that the compositions of *m*- and *p*-CNB are not different between the two locations at the different temperature. Thus, the composition gradient does not occur during the experiment.

However, even the temperature gradient was not studied in this experiment. Its effect could be indirectly drawn from Tables 4.4 and 4.5. The composition of *p*-CNB in the precipitate far from the zeolite is lower than that near the zeolite. It may be because there is a heat transfer from the wall to the center of the crystallizer. The crystallizer was designed as a double-glassed layer, and its temperature was controlled by cooling water flowing between the glass layers (Figure 4.41). The location near the wall could have slightly lower temperature than the location near the zeolite, resulting in the faster formation and agglomeration of the precipitate in this area. The faster the precipitate forms, the lower the purity of the precipitate. That is due to the inclusion of mother liquor into the precipitates (Funakoshi *et al.*, 2000; Takiyama *et al.*, 2001). This could be a reason for the lower

p-CNB composition in the precipitate in area (b). Nevertheless, in order to confirm the hypothesis, further experiment should be studied on the temperature gradient by measuring the temperature difference of the mixture at the position along the radius of the crystallizer.

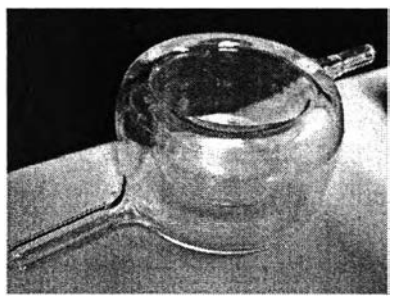

Figure 4.41 Crystallizer.

From this study, it could be concluded that the composition of the *p*-CNB in the precipitates partly depends on the position of the precipitate and the type of the zeolite and also possibly relies on the temperature gradient.